doi:10.1088/0004-637X/741/1/23

POSSIBLE EVIDENCE FOR A FISK-TYPE HELIOSPHERIC MAGNETIC FIELD. I. ANALYZING *ULYSSES*/KET ELECTRON OBSERVATIONS

O. Sternal, N. E. Engelbrecht[1], R. A. Burger[1], S. E. S. Ferreira[1], H. Fichtner[2], B. Heber, A. Kopp, M. S. Potgieter[1], and K. Scherer[2]

Institut für Experimentelle und Angewandte Physik, Christian-Albrechts-Universität zu Kiel, Leibnizstr. 11, 24118 Kiel, Germany; oliver.sternal@rub.de

Received 2011 March 31; accepted 2011 July 26; published 2011 October 12

ABSTRACT

The propagation of energetic charged particles in the heliospheric magnetic field is one of the fundamental problems in heliophysics. In particular, the structure of the heliospheric magnetic field remains an unsolved problem and is discussed as a controversial topic. The first successful analytic approach to the structure of the heliospheric magnetic field was the Parker field. However, the measurements of the *Ulysses* spacecraft at high latitudes revealed the possible need for refinements of the existing magnetic field model during solar minimum. Among other reasons, this led to the development of the Fisk field. This approach is highly debated and could not be ruled out with magnetic field measurements so far. A promising method to trace this magnetic field structure is to model the propagation of electrons in the energy range of a few MeV. Employing three-dimensional and time-dependent simulations of the propagation of energetic electrons, this work shows that the influence of a Fisk-type field on the particle transport in the heliosphere leads to characteristic variations of the electron intensities on the timescale of a solar rotation. For the first time it is shown that the *Ulysses* count rates of 2.5–7 MeV electrons contain the imprint of a Fisk-type heliospheric magnetic field structure. From a comparison of simulation results and the *Ulysses* count rates, realistic parameters for the Fisk theory are derived. Furthermore, these parameters are used to investigate the modeled relative amplitudes of protons and electrons, including the effects of drifts.

Key words: cosmic rays – diffusion – magnetic fields – Sun: heliosphere

Online-only material: color figures

1. INTRODUCTION

The transport of energetic charged particles through the heliosphere is one of the fundamental processes investigated in heliophysics. Parker (1965) derived a transport equation (TPE) describing the time evolution of an isotropic particle distribution under the influence of four basic physical processes: diffusion and drift in the heliospheric magnetic field (HMF), convection with the solar wind (SW), and adiabatic energy changes. The main problems in solving this partial differential equation involve large uncertainties in the parameters.

The first successful theoretical approach to the global structure of the HMF was proposed by Parker (1958), suggesting the field lines to be structured as Archimedean spirals. However, the measurements of the first out-of ecliptic spacecraft *Ulysses* revealed that the particle count rates at high heliographic latitudes could not be reproduced using the standard diffusion parameters that were at that time accepted to be correct (Simpson et al. 1995a, 1995b; Ferrando 1999). It was shown that the diffusion in polar direction is considerably higher in the fast SW during solar minimum than assumed so far (Jokipii et al. 1995).

Among other reasons, like the observation of latitudinal field components close to the Sun and a rigid rotation of coronal holes, this leads to the suggestion of a different and more complex model of the HMF (Fisk 1996). This new approach proposed magnetic field lines connecting the equatorial regions of the heliosphere with the polar regions, allowing energetic particles to travel more easily in the polar direction along the magnetic field lines.

However, the existence of such a Fisk-type HMF structure is discussed controversially (Lionello et al. 2006; Roberts et al. 2007; Burger et al. 2008) and magnetic field measurements did not find the predicted signatures (Forsyth et al. 2002; Roberts et al. 2007). However, investigating the original Fisk field, Roberts et al. (2007) found an upper limit for the Fisk field parameters to be significantly lower than expected by Zurbuchen et al. (1997). The existence of a Fisk-type field with a smaller Fisk effect, as, e.g., proposed by Hitge & Burger (2010), still remains an open possibility. Applying an MHD model, Lionello et al. (2006) could confirm Fisk's idea of the HMF, but found the Fisk field parameters assumed so far to be highly overestimated. Burger et al. (2008) argue that the azimuthal component of the Parker field is inversely proportional to the SW speed so that significant periodicities are expected to be found. The analysis of Roberts et al. (2007) suggested that these are also not observed. Therefore, Burger et al. (2008) question the possibility of observing the periodicities predicted by the Fisk field in the inner heliosphere and explain that these periodicities could be masked by other effects. If this were indeed the case, the only means of investigating the HMF structure in the inner heliosphere would necessarily be indirect. Particle propagation is very sensitive to the HMF structure, since the magnetic field influences the motion of charged particles to a large extent. For this reason, simulations of the electron propagation within the heliosphere and their comparison with spacecraft measurements give the opportunity to contribute to the open question of the global HMF structure via a remote sensing method.

A promising approach to find less ambiguous signatures of a Fisk-type HMF is the investigation of electrons at energies of a few MeV, where drift effects are negligible (see, e.g., Potgieter 1996; Potgieter & Ferreira 1999). Two dominant particle sources are known: galactic and Jovian electrons. In this contribution,

[1] Center for Space Research, North-West University, 2520 Potchefstroom, South Africa.

[2] Institut für Theoretische Physik, Lehrstuhl IV: Weltraum- und Astrophysik, Ruhr-Universität Bochum, 44780 Bochum, Germany.

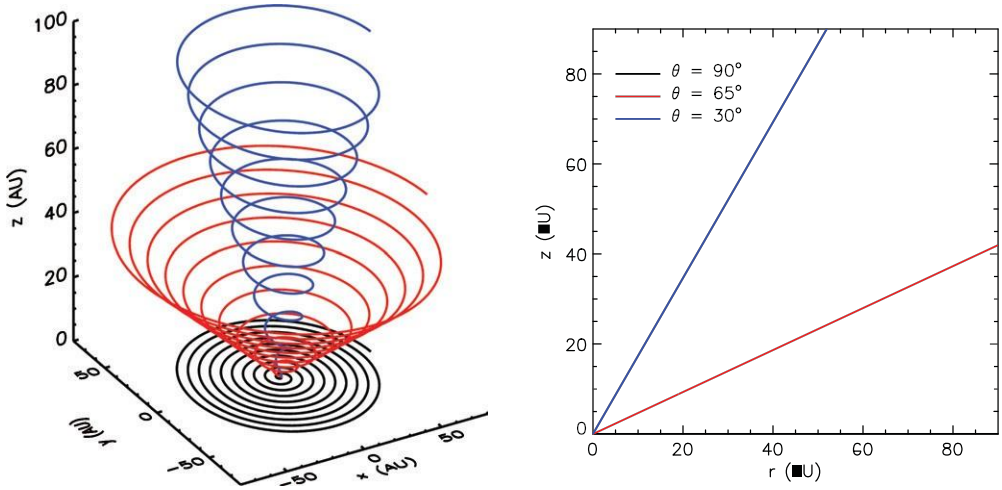

Figure 1. Two different visualizations of three field lines of the Parker field.
(A color version of this figure is available in the online journal.)

we present time-dependent numerical simulations of the low-energy electron flux in the heliosphere. The computed electron intensities are compared to the observations of the *Ulysses* spacecraft. It is shown that the *Ulysses* count rates of 2.5–7 MeV electrons contain time variations caused by the imprint of a Fisk-type HMF structure. From a comparison of our model computations and the *Ulysses* observations, correspondingly consistent parameter values for the Fisk theory are derived. Lastly, comparisons are made between the relative amplitudes for galactic protons, electrons, and Jovians yielded by the Potchefstroom three-dimensional steady-state code, using a Schwadron–Parker field with the more realistic values of the above-mentioned parameters, to ascertain the effects of cosmic-ray drift and the inclusion of a Jovian source.

2. THE HELIOSPHERIC MAGNETIC FIELD STRUCTURE DURING SOLAR MINIMUM

Parker (1958) developed a simple and very successful model describing the global structure of the HMF as Archimedean spirals on cones, a concept supported by spacecraft observations in the ecliptic plane (Ness & Burlaga 2001, and references therein). The magnetic field vector in spherical coordinates (r, θ, φ) is given by

$$B = B_e \frac{r_e^2}{r^2} \left[e_r - \frac{\Omega_S (r - r_{ss}) \sin\theta}{u_{sw}} e_\varphi \right] \qquad (1)$$

with B_e and r_e to indicate the normalization at Earth's orbit, the SW speed u_{sw}, the radius of the source surface r_{ss}, and the solar rotation rate Ω_S. To visualize the structure of the Parker field, Figure 1 presents two plots of the corresponding field lines. The upper panel shows a three-dimensional illustration of three field lines. Their footpoints share the same longitude, but are located at different colatitudes: $\theta_{black} = 90^\circ$, $\theta_{red} = 65^\circ$, and $\theta_{blue} = 30^\circ$ from the solar north pole. The spirals form cones with fixed colatitudes. The right panel displays the same field lines in an unwound projection with the field line altitude z above the equatorial plane versus the radial distance $r = \sqrt{x^2 + y^2}$. In this representation the field lines appear as straight lines with fixed colatitudes.

Particles accelerated at corotating interaction regions (CIRs) can be measured in the ecliptic plane with a period of ~26 days. In a Parker-type HMF these particles are expected to stay at low heliographic latitudes (Gosling & Pizzo 1999). However, the first *Ulysses* fast latitude scan (FLS) discovered 26 day variations even at the highest latitudes (Simpson et al. 1995a; Kunow et al. 1995; Dunzlaff et al. 2008). Another result of *Ulysses*' first FLS was that the latitudinal gradient of the particle measurements is significantly lower than expected from a Parker HMF model (Simpson et al. 1996; McKibben et al. 1996).

Two theories were developed to explain these surprising measurements. Kóta & Jokipii (1995) introduced a large cross-field diffusion coefficient at higher latitudes during the solar minimum phase motivated by large turbulence in the fast SW. Fisk (1996) chose a different approach to describe the HMF during solar minimum conditions. He developed an HMF model allowing magnetic field lines to wander in colatitude. Energetic particles can diffuse easily along these field lines and reach the polar region to cause the variations mentioned above. Considering the tilt between the rotational and magnetic symmetry axis of the Sun, the differential rotation of the photosphere and a non-radial expansion of magnetic field lines from the photosphere to the source surface, Zurbuchen et al. (1997) derived the magnetic field vector of such an HMF in a corotating frame to be

$$\begin{aligned} B_r &= B_e \left(\frac{r_e}{r} \right)^2 \\ B_\theta &= \frac{B_e r_e^2}{u_{sw} r} \omega \sin\beta \sin\left[\varphi + \frac{r\Omega_S}{u_{sw}} - \varphi_0 \right] \\ B_\varphi &= \frac{B_e r_e^2}{u_{sw} r} \left[\omega \left(\cos\beta \sin\theta + \sin\beta \cos\theta \right) \right. \\ &\quad \left. \times \cos\left[\varphi + \frac{r\Omega_S}{u_{sw}} - \varphi_0 \right] - \Omega_S \sin\theta \right] \end{aligned} \qquad (2)$$

with ω the differential rotation rate of the Sun and β the Fisk angle, defined as the angle between the Sun's rotational axis and the line tangent to the field line connecting the source surface to the solar pole (for details see Fisk 1996). Following the study of Zurbuchen et al. (1997), most investigations regarding the Fisk field employed $\beta = 30^\circ$.

The Fisk field can only by valid in the fast SW originating from the polar coronal holes (PCHs). A different behavior of the footpoint motion is expected at the boundaries of the PCHs and

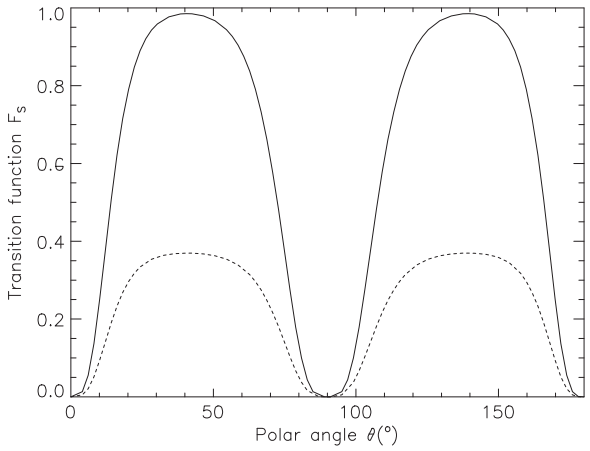

Figure 2. Full transition function (solid line) following Equation (3) and a reduced transition function (dashed line) used in the parameter study presented in Section 5.

outside of the coronal holes. Schwadron & McComas (2003) derived a description of the Fisk field allowing the SW speed to depend on the heliographic colatitude θ. This is commonly referred to as the Schwadron field. Burger & Hitge (2004) proposed a Fisk–Parker hybrid HMF model. They implemented a transition function F_S depending on the latitude to build up a pure Parker field in the equatorial region and a Fisk field at higher latitudes in the PCHs. Assuming no differential rotation at the highest latitudes (Schou et al. 1998), the field becomes again Parker-like in the polar regions. This function is given by

$$F_S(\theta) = \begin{cases} \tanh(\delta_p\theta) + \tanh(\delta_p[\theta-\pi]) \\ \quad -\tanh\left(\delta_e\left[\theta-\theta_b\right]\right)^2, & 0 \quad \theta < \theta_b \\ 0, & \theta_b \quad \theta < \pi-\theta_b \\ \tanh(\delta_p\theta) + \tanh(\delta_p[\theta-\pi]) \\ \quad -\tanh(\delta_e[\theta-\pi+\theta_b])^2, & \pi-\theta_b \quad \theta < \pi \end{cases} \quad (3)$$

with the PCH boundary on the source surface described by θ_b and two parameters δ_p and δ_e controlling the shape of the transition function. When F_S is equal to one, the HMF is most Fisk-like, while a value of zero reduces the field to a standard Parker spiral (solid line in Figure 2). Burger et al. (2008) extended this model to describe its time dependence during the solar activity cycle and on short timescales.

Hitge & Burger (2010) presented a combination of the field models introduced by Schwadron & McComas (2003) and Burger & Hitge (2004). In a fixed frame, this field is given by

$$\begin{aligned} B_r &= B_e\left(\frac{r_e}{r}\right)^2\left(1+\frac{r}{u_{sw}^2}\omega^*\sin\beta^*\sin\varphi^*\frac{du_{sw}}{d\theta}\right) \\ B_\theta &= \frac{B_e r_e^2}{u_{sw} r}\omega^*\sin\beta^*\sin\varphi^* \\ B_\varphi &= \frac{B_e r_e^2}{u_{sw} r}(\sin\theta(\omega^*\cos\beta^*-\Omega_S) \\ &\quad + \frac{d}{d\theta}(\omega^*\sin\beta^*\sin\theta)\cos\varphi^*) \end{aligned} \quad (4)$$

with

$$\begin{aligned} \beta^*(\theta) &= \beta F_S(\theta) \\ \omega^*(\theta) &= \omega F_S(\theta) \\ \varphi^* &= \varphi - \Omega_S t + \frac{\Omega_S}{u_{sw}}(r-r_{SS}) + \varphi_0. \end{aligned}$$

In what follows, this HMF model is referred to as the Schwadron–Parker hybrid field. Note that Hitge & Burger (2010) used $\varphi^* = \varphi + \frac{\Omega_S}{u_{sw}}(r-r_{SS}) + \varphi_0$, while in this work we employ φ^* from Burger et al. (2008) to introduce the time dependence on timescales of the solar rotation into the HMF model. The solar cycle dependence of the model parameters is discussed in detail by Burger et al. (2008). Depending on the tilt angle, they expect the Fisk angle β to vary between 0° (solar maximum) and ∼25° (around solar minimum) during the 11 year cycle.

Figure 3 illustrates the complexity of this HMF model. The upper panel shows the three-dimensional structure of the Schwadron–Parker field for two field lines with different initial colatitudinal positions of their footpoints (black line: $\theta_0 = 90°$, blue line: $\theta_0 = 30°$ from the solar north pole). In the equatorial region the HMF is a Parker spiral, while the field structure

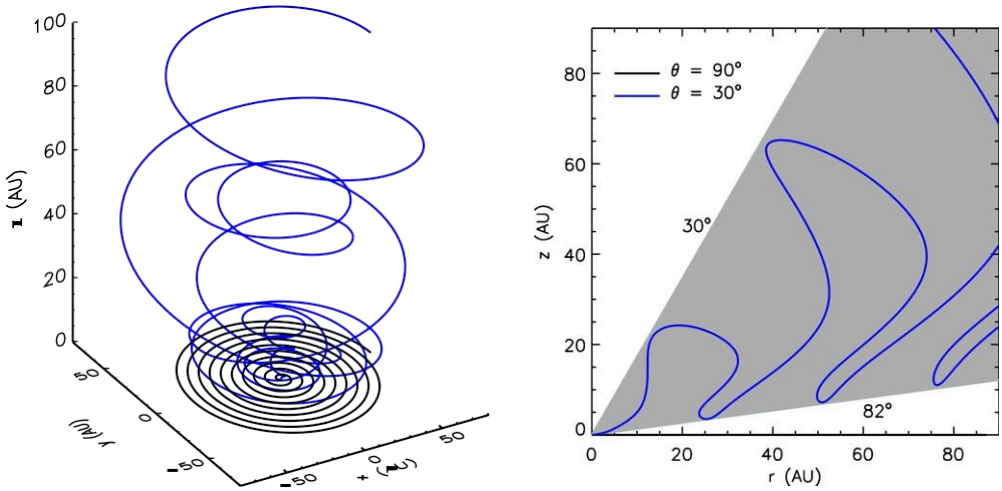

Figure 3. Two different visualizations of two field lines of the Schwadron–Parker hybrid field.
(A color version of this figure is available in the online journal.)

becomes more complicated at higher latitudes. The lower panel displays an unwound projection of the same field lines. The wavy structure of the high latitude field line connecting wide latitudinal ranges of the heliosphere (gray area) becomes evident. For a comparison of the different HMF models, see the recent paper by Scherer et al. (2010).

3. PARTICLE TRANSPORT IN THE HELIOSPHERE

The propagation of cosmic rays within the heliosphere is described by the Parker TPE (Parker 1965) and is discussed in detail, e.g., by Potgieter (1998):

$$\frac{\partial f}{\partial t} = \underbrace{\nabla \cdot (\hat{\kappa} \cdot \nabla f)}_{\text{diffusion}} - \underbrace{(u_{sw} + v_D) \cdot \nabla f}_{\text{convection and drift}} + \underbrace{\frac{1}{3}(\nabla \cdot u_{sw}) \frac{\partial f}{\partial (\ln P)}}_{\text{adiabatic energy changes}} + \underbrace{S}_{\text{sources}} . \quad (5)$$

Parker's TPE describes the temporal evolution of the pitch-angle isotropic differential cosmic-ray distribution function $f(r, P, t)$ depending on the position r in the heliosphere, the particle rigidity P, and the time t. It takes into account the four basic physical processes influencing the particle's distribution function: convection with the SW speed u_{sw}, particle drifts with the drift velocity v_D, diffusion described by the diffusion tensor $\hat{\kappa}$ in a coordinate system aligned with the underlying magnetic field and adiabatic energy changes. Particle sources and sinks are included in the TPE via the term S.

The drift velocity can be expressed in terms of a drift coefficient κ_A:

$$v_D = \nabla \times (\kappa_A e_B) \quad (6)$$

and, therefore, can be included in the diffusion tensor:

$$\hat{\kappa} = \begin{bmatrix} \kappa & 0 & 0 \\ 0 & \kappa_{\perp r} & \kappa_A \\ 0 & -\kappa_A & \kappa_{\perp \theta} \end{bmatrix} . \quad (7)$$

For further computations this tensor has to be transformed to spherical polar coordinates:

$$\hat{\kappa}_{\text{sphere}} = \begin{bmatrix} \kappa_{rr} & \kappa_{r\theta} & \kappa_{r\varphi} \\ \kappa_{\theta r} & \kappa_{\theta\theta} & \kappa_{\theta\varphi} \\ \kappa_{\varphi r} & \kappa_{\varphi\theta} & \kappa_{\varphi\varphi} \end{bmatrix} . \quad (8)$$

This conversion is given by Burger et al. (2008):

$$\begin{aligned}
\kappa_{rr} &= \kappa_{\perp\theta} \sin^2\zeta + \cos^2\zeta (\kappa \cos^2\psi + \kappa_{\perp r} \sin^2\psi) \\
\kappa_{r\theta} &= -\kappa_A \sin\psi + \sin\zeta \cos\zeta \\
&\quad \times (\kappa \cos^2\psi + \kappa_{\perp r} \sin^2\psi - \kappa_{\perp\theta}) \\
\kappa_{r\varphi} &= -\kappa_A \cos\psi \sin\zeta - (\kappa - \kappa_{\perp r}) \sin\psi \cos\psi \cos\zeta \\
\kappa_{\theta r} &= \kappa_A \sin\psi + \sin\zeta \cos\zeta \\
&\quad \times (\kappa \cos^2\psi + \kappa_{\perp r} \sin^2\psi - \kappa_{\perp\theta}) \\
\kappa_{\theta\theta} &= \kappa_{\perp\theta} \cos^2\zeta + \sin^2\zeta (\kappa \cos^2\psi + \kappa_{\perp r} \sin^2\psi) \\
\kappa_{\theta\varphi} &= \kappa_A \cos\psi \cos\zeta - (\kappa - \kappa_{\perp r}) \sin\psi \cos\psi \sin\zeta \\
\kappa_{\varphi r} &= \kappa_A \cos\psi \sin\zeta - (\kappa - \kappa_{\perp r}) \sin\psi \cos\psi \cos\zeta \\
\kappa_{\varphi\theta} &= -\kappa_A \cos\psi \cos\zeta - (\kappa - \kappa_{\perp r}) \sin\psi \cos\psi \sin\zeta
\end{aligned}$$

with

$$\tan\psi = -\frac{B_\varphi}{\sqrt{B_r^2 + B_\theta^2}} \quad \text{and} \quad \tan\zeta = \frac{B_\theta}{B_r}.$$

In this work, we employ the diffusion tensor described by, e.g., Ferreira et al. (2001a):

$$\begin{aligned}
\kappa &= \kappa_0 \frac{v}{c} f_1(r, P) \\
\kappa_{\perp r} &= a \cdot \kappa \\
\kappa_{\perp\theta} &= b \cdot \kappa .
\end{aligned} \quad (10)$$

Here, v and c denote the particle speed and the speed of light, respectively, and $\kappa_0 = 4.5 \times 10^{18}\,\mathrm{m^2\,s^{-1}}$. See Ferreira et al. (2001a, 2001b) or Ferreira et al. (2003) for a detailed discussion of the spatial and energy dependence of κ and the ratios a and b of the perpendicular diffusion coefficients. Since our investigation concentrates on 7 MeV electrons, drift effects are neglected ($\kappa_A = 0$).

The current work employs a refined version of the VLUGR3-based model developed by Fichtner et al. (2001). VLUGR3 (Blom & Verwer 1994, 1996) solves partial differential equations of the form

$$F\left(t, \{x_i\}, f, \frac{\partial f}{\partial x_i}, \frac{\partial^2 f}{\partial x_i x_j}\right) = 0 \quad (11)$$

with the time t, the three Cartesian coordinates x_i, and the function f. Since it is not possible to solve the full three-dimensional TPE also in energy with this code, it is necessary to derive a simplification of the partial differential equation because of the rigidity-dependent adiabatic term. Therefore, following an idea by Drury & Völk (1981), Fichtner et al. (2001) employed the second moment of the distribution function

$$P_e = \frac{4\pi}{3} \int_0^\infty f(r, p, t)\, p v p^2 dp \quad (12)$$

with the particle speed v. Neglecting the drift term, this approach leads to a hydrodynamic formulation of the TPE:

$$\begin{aligned}
\frac{\partial P_e}{\partial t} &= \nabla \cdot (\hat{\kappa} \cdot \nabla P_e) - u_{sw} \cdot \nabla P_e \\
&\quad - \frac{4}{3}(\nabla \cdot u_{sw}) P_e + S .
\end{aligned} \quad (13)$$

Here, $\hat{\kappa}$ and S denote the momentum-averaged diffusion tensor and source term, respectively. However, in the model the diffusion tensor is evaluated at $E = 7$ MeV, the energy of interest to this study. The resulting P_e shows the same time and space variations as the phase space distribution f in Parker's TPE: Kissmann (2002) tested the time-dependent simplified VLUGR3-based model against the South African steady-state code (Ferreira et al. 2001a, 2001b) and found a qualitative agreement in the results. This model has been employed successfully by, e.g., Fichtner et al. (2001), Kissmann et al. (2003, 2004), and Lange et al. (2006). Therefore, the Fichtner model is very useful for the investigation of the time-dependent behavior of the low-energy electron flux in the

$$\kappa_{\varphi\varphi} = \kappa \sin^2 \psi + \kappa_{\perp r} \cos \psi \quad (9)$$

heliosphere.

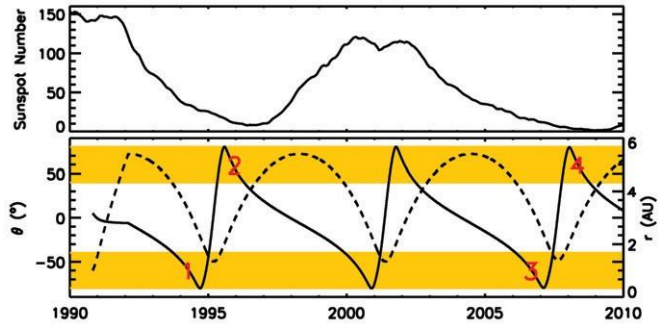

Figure 4. Smoothed sunspot number (upper panel) and the *Ulysses* trajectory (lower panel, solid line: heliographic latitude, dashed line: radial distance to the Sun).

(A color version of this figure is available in the online journal.)

4. ANALYSIS OF MODEL RESULTS AND *ULYSSES*/KET DATA

4.1. 26 day Variations of Low-energy Electrons

The implementation of a Fisk-type HMF in numerical models simulating particle transport in the HMF by solving Parker's TPE is very complex and has up to now been limited to steady-state models (see, e.g., Burger & Hitge 2004; Miyake & Yanagita 2008; Burger et al. 2008; Engelbrecht & Burger 2010). Employing the VLUGR3-based model, we can investigate the time-dependent behavior of the electron flux at low energies in a Fisk-type field. We computed the 7 MeV electron flux along the *Ulysses* trajectory in a Schwadron–Parker hybrid field including galactic and Jovian electrons. The computations were carried out in a fixed frame with a time-dependent magnetic field. For our investigation, we use the galactic electron spectrum from Langner et al. (2001) as the boundary spectrum at 100 AU and the Jovian electron spectrum from Ferreira et al. (2001a). The HMF parameters used in Equation (4) are $\delta_p = 5.0$, $\delta_e = 5.0$, $\theta_b = 80^\circ$, $\Omega_S = 26$ day^{-1}, $\omega = \Omega_S/4$, and $\beta = 30^\circ$. The SW speed was chosen to be 400 km s^{-1} around the ecliptic and 800 km s^{-1} at higher latitudes. For this representation of the HMF, the influence of the Fisk-type HMF structure on the electron intensities is expected to become strongest for the PCHs at latitudes between 80° and 40°.

As shown in Figure 4, *Ulysses* investigated the latitudinal range of interest (yellow shaded areas in the lower panel) several times. However, the FLSs are too short to derive a meaningful longitudinal variation of the low-energy electron flux. Additionally, a Fisk-type HMF is only expected to exist during solar minimum conditions (compare upper panel). Therefore, in principle only four potential periods fulfill the requirements of our investigation and are marked 1–4 in the lower panel of Figure 4. Unfortunately, during period four the data coverage of *Ulysses*/Kiel Electron Telescope (KET) became too low for an adequate analysis. The time periods one and three have been analyzed by Kunow et al. (1995) and Zhang et al. (1995), as well as by Lario & Roelof (2007) and Dunzlaff et al. (2010), respectively. These authors find CIRs to lead to recurrent particle events and cosmic ray decreases during these time periods. Hence, the influence of the HMF structure may be masked by other interplanetary phenomena. During the second potential period from 1995.6 to 1996.3, Heber et al. (1997) and Kunow et al. (1999) could show that CIR particle events and CIR related cosmic ray decreases were first observed from 1996.0 onward. The left panel of Figure 5 presents the expected detrended 7 MeV electron intensities yielded by the model along the *Ulysses* trajectory when the spacecraft was located between 80° N and 40° N heliographic latitude. The computed electron flux reveals a clear variation of up to ∼50% around the running mean due to the HMF configuration. The right panel shows the corresponding Lomb frequency analysis (Lomb 1976) with the 90% (lower dashed line) and 99% (upper dashed line) significance levels. A Schwadron–Parker hybrid HMF leads to strong variations with a periodicity of 26 days. The next step is to investigate the *Ulysses* electron observations for a periodic 26 day signal.

The variation of the *Ulysses*/KET electron data from 1995.6 to 1996.3 is displayed in Figure 6. During the considered time span, the spacecraft moved from 80° north to 40° north, the latitudes where the influence of a Fisk-type HMF should be most pronounced during solar minimum conditions. The upper panel presents the deviation from the running mean of the electron count rate with a mean value of the deviation of 37%. To guide the eye, a sine wave with a periodicity of 26 days is plotted over the observations (dashed blue line). Lomb frequency analyses were performed of different subsets of the time period from 1995.6 to 1996.3. The results are displayed in the lower panels of Figure 6 with the upper and lower dashed lines indicating the 99% and the 90% significance levels, respectively. For all three cases, a periodicity of 26 days is found with the power of the

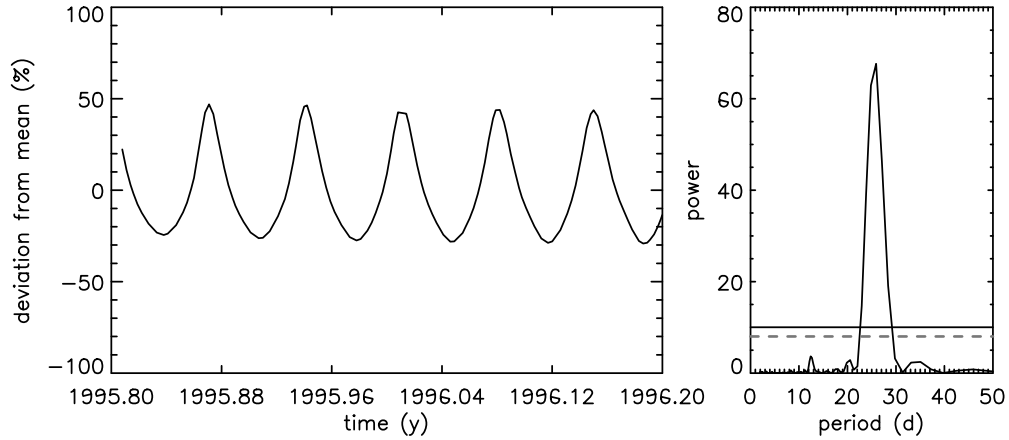

Figure 5. Detrended electron flux (model computation) along the *Ulysses* trajectory at high heliographic latitudes (left panel) employing a Schwadron–Parker hybrid HMF with $\beta = 30^\circ$ and the corresponding Lomb frequency analysis (right panel).

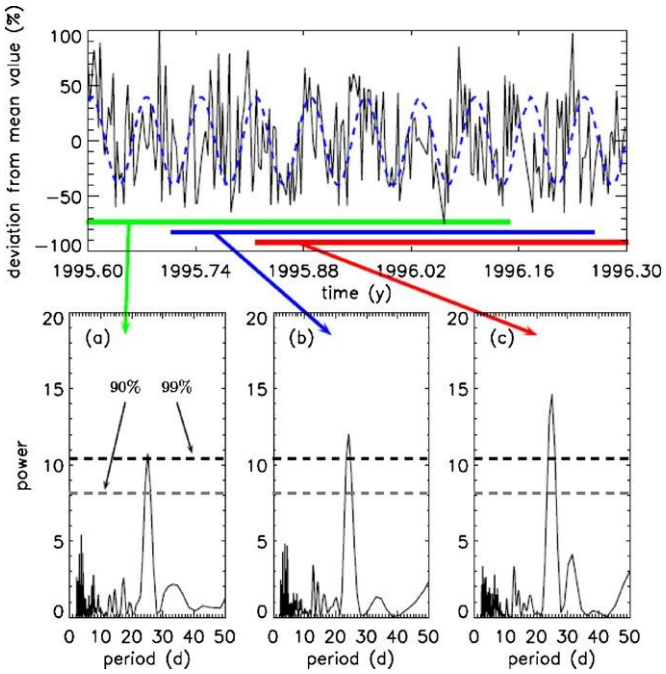

Figure 6. Detrended 2.5–7 MeV electron count rates measured by *Ulysses*/KET at the highest northern heliographic latitudes (upper panel) and the corresponding Lomb frequency analyses (lower panels).
(A color version of this figure is available in the online journal.)

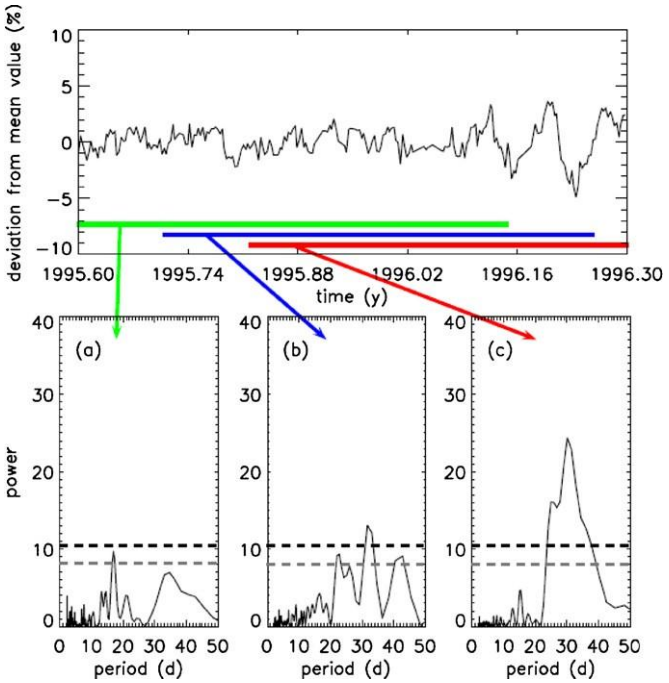

Figure 7. Same as Figure 6, but for 250–2000 MeV protons. (A color version of this figure is available in the online journal.)

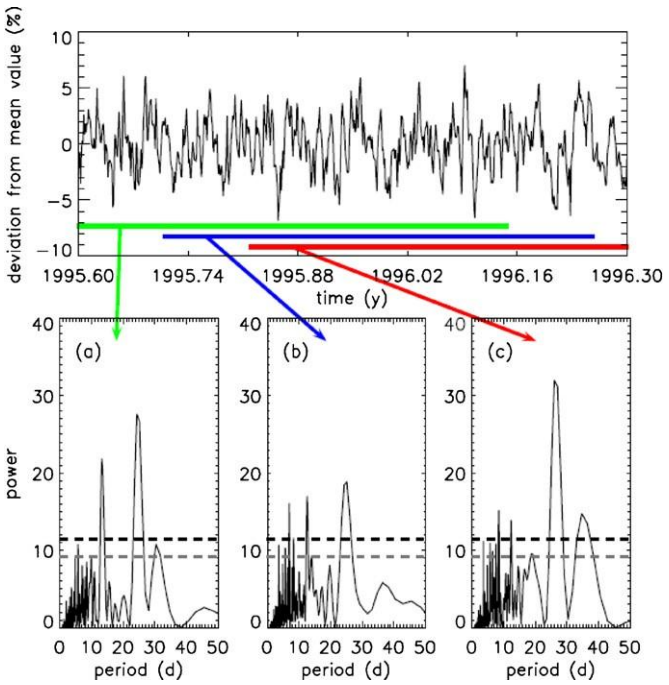

Figure 8. Same as Figure 6, but for the solar wind speed measured by *Ulysses*/SWOOPS.
(A color version of this figure is available in the online journal.)

periodicity lying above the 99% significance level (black dashed line). The periodicity in the electron count rates gets stronger toward lower latitudes (panels (b) and (c)), but is, however, detectable up to the highest latitudes (panel (a)) accessible to the spacecraft.

4.2. Independence of CIRs and SW Speed Variations

To assure that these 26 day variations can indeed be produced by a Fisk-type HMF, it is necessary to eliminate the possibility that they are caused by CIRs. Hence, the *Ulysses*/KET measurements of 250–2000 MeV protons are investigated for a correlation with the electron count rate. This study is shown in Figure 7. The upper panel displays the deviation from the running mean of the proton count rate. During most of the measurement, little periodic behavior is visible. Only after ∼1996.1, when *Ulysses* approaches low latitudes, do fluctuations appear in the proton count rate. This becomes evident in the Lomb analyses (lower panels) for different subsets of the measurements. At the highest latitudes (panel (a)), the protons reveal a periodicity of ∼15 days, while they show a variation with a periodicity >30 days at lower latitudes (panels (b) and (c)). A periodicity of 26 days only appears in panel (c), where the measurements after 1996.1 are fully taken into account.

An additional possible source of the electron variations can be found in the SW. Therefore, an analysis of the SW speed is performed. The upper panel of Figure 8 displays the detrended deviation of the daily averaged SW speed measured by *Ulysses*/SWOOPS from 1995.6 to 1996.3 with an average deviation of 2.4%. The lower panels present the Lomb analyses of different subsets of this time period. All three panels reveal a 26 day variation in the SW speed with a power above the 99% significance level. This leads to the question of whether the electron variations are related to the SW speed variations.

To achieve a deeper insight into these possible correlations, the Pearson correlation coefficient

$$\mathrm{cor}\,(x, y) = \frac{\sum_{i=1}^{n} (x_i - \bar{x})(y_i - \bar{y})}{\sum_{i=1}^{n} (x_i - \bar{x})^2 \cdot \sum_{i=1}^{n} (y_i - \bar{y})^2} \qquad (14)$$

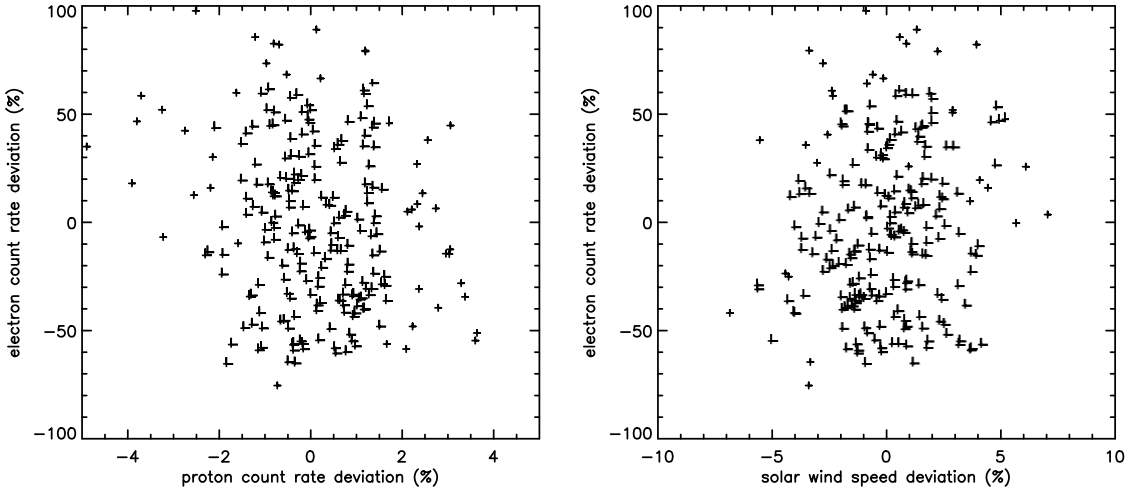

Figure 9. Test for a correlation between the *Ulysses* electron count rate and the proton count rate or the solar wind speed.

Table 1
Overview of the Electron Data Lomb Analyses, the Electron–Proton Correlation (e–p), and the Electron–Solar Wind Speed Correlation (e–u_{sw})

Period	Max. Power	e–p	e–u_{sw}
(a)	10.75	−0.11	0.22
(b)	12.02	−0.10	0.16
(c)	14.64	−0.21	0.11

with $\mathrm{cor}\,(x, y) \in [-1, 1]$ is computed for the electron and proton count rates, as well as the electron count rate and the SW speed. Here, x and y denote the electron and proton/SW speed data arrays, respectively, and

$$x = \frac{1}{n}\sum_{i=1}^{n} x_i \quad \text{and} \quad y = \frac{1}{n}\sum_{i=1}^{n} y_i \qquad (15)$$

are the corresponding mean values. Depending on the result of the function, a decision can be made whether a correlation between the two measurements exists:

$$\mathrm{cor}\,(x, y) = \begin{cases} 1 & \text{correlation} \\ 0 & \text{no correlation} \\ -1 & \text{anti-correlation.} \end{cases}$$

The correlation coefficient is computed for the corresponding time periods discussed in Figures 6–8 and is presented in Table 1 together with the maximum power of the 26 day period of the electron count rate taken from the Lomb analysis. The correlation coefficient yields low negative values for the electron–proton correlation for all chosen subsets of the data, only beginning to increase when the lowest latitudes of the utilized measurements are taken into account. Following this analysis, the conclusion is obvious that the electrons and protons are not correlated and behave independently at mid to high latitudes. This can also be deduced from Figure 9. The upper panel shows the data points of the deviation from the running mean of the electron count rate plotted over the corresponding data points of the deviation of the detrended proton count rate. If there was a correlation between these two data sets, a regular pattern of the data point distribution would be expected. This is, however, not the case.

The SW speed analysis leads to a similar situation. The correlation coefficient yields low positive values for all subsets of the measurement, rising toward higher latitudes. However, the correlation coefficient of the electron count rate and the SW speed is too low to indicate a correlation. This is supported by the lower panel of Figure 9. The data points of the deviation from the running mean of the electron count rate are plotted over the corresponding data points of the deviation of the detrended SW speed. Again, no regular pattern appears in the data point distribution, indicating that no correlation can be found between the electron count rate and the SW speed.

For a comparison with the current study, the time span analyzed by Heber et al. (1997) is re-investigated for a correlation between the 250–2000 MeV proton count rate and the SW speed. These authors find recurrent variations in the proton count rate and relate them to the SW speed variations. This analysis is shown in Figure 10. The upper left panel displays the detrended deviations of the proton count rate (red line) and the SW speed (black line) from their respective mean values between 1996.1 and 1996.4. The recurrent and anti-correlated variations become evident. The upper right panel presents the corresponding Lomb analysis with the same color coding. The dashed lines represent the 99% significance levels. For both measurements, the Lomb analysis reveals a strong periodicity with the same duration. The lower panel shows the detrended deviation of the proton count rate plotted over the corresponding data points of the SW speed deviation arranged close to the corresponding regression line, which was added to the plot to guide the eye. The correlation coefficient yields a value of −0.58 for these measurements. In contrast to the investigation of a possible electron–proton or electron–SW speed correlation, this study suggests a possible correlation between the proton count rate and the SW speed (see also Heber et al. 1997).

Based on this investigation, we assume the HMF structure to be the cause of the 26 day variations found in the *Ulysses* electron count rates. Further assuming that the structure of the HMF is described by a Fisk-type HMF model, i.e., the Schwadron–Parker field (Hitge & Burger 2010), implications on the parameters describing the field structure can be deduced from the *Ulysses*/KET electron measurements.

5. DEDUCING HMF PARAMETER VALUES FROM ELECTRON SIMULATIONS AND *ULYSSES* MEASUREMENTS

Following the assumption that the 26 day variation found in the *Ulysses*/KET electron data is caused by a Fisk-type HMF,

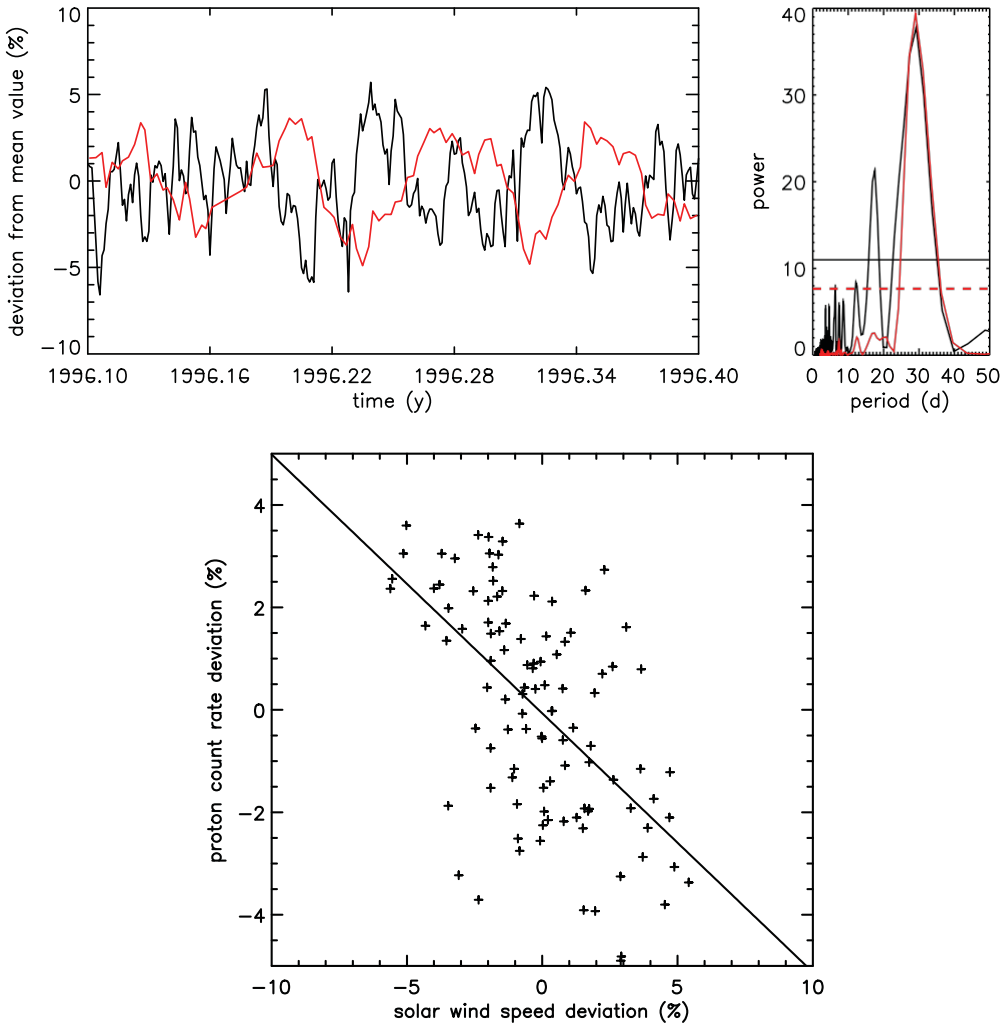

Figure 10. Correlation of the proton count rate and the solar wind speed between 1996.1 and 1996.4.
(A color version of this figure is available in the online journal.)

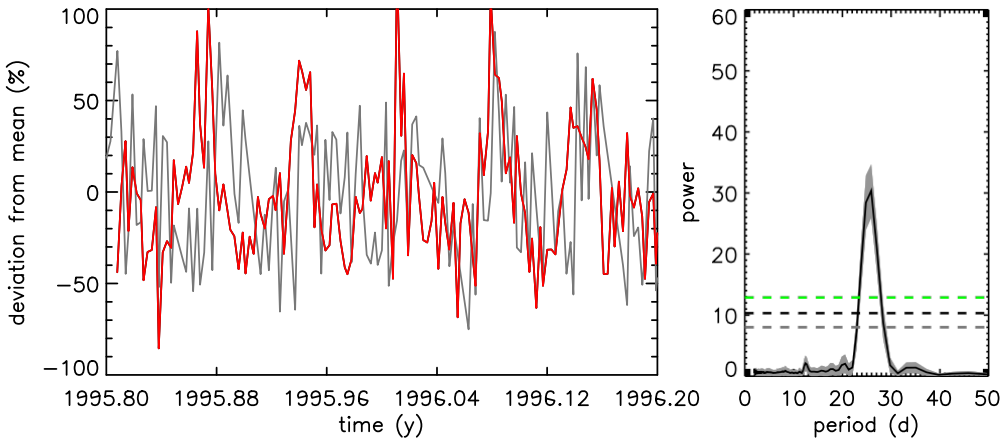

Figure 11. Same as Figure 5, but with white noise added to the model data.
(A color version of this figure is available in the online journal.)

consequences for the Fisk theory can be derived by comparing the model data of the 7 MeV electron count rate with *Ulysses* measurements. To achieve a realistic comparison of the model data with the observations, one has to take into account that the measurements are limited in their precision due to counting statistics. The distribution can be approximated by Poisson statistics resulting in a white noise component present in the Lomb spectra. The left panel of Figure 11 displays the same model data as Figure 5, but with additional white noise computed from the Poisson statistics of *Ulysses*/KET (red curve) and added to the model data with the Box–Muller method (Box & Muller 1958). The gray line shows the *Ulysses*/KET electron

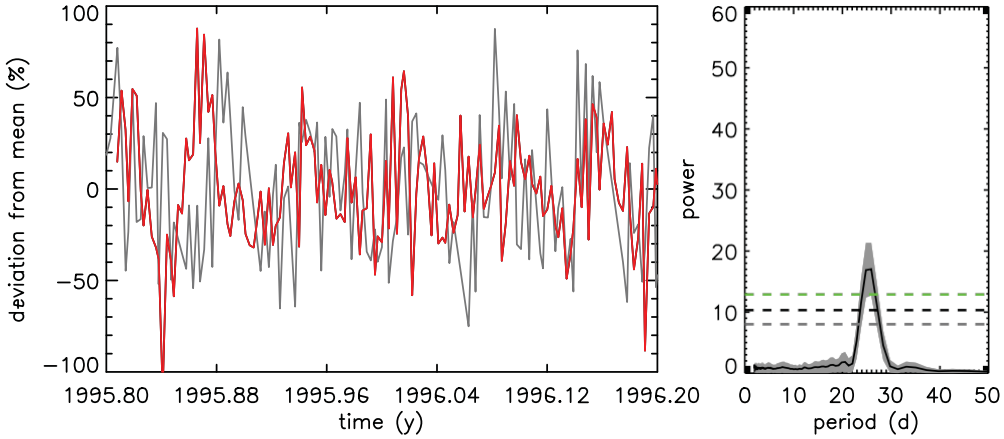

Figure 12. Same as Figure 11, but with $\beta = 6^{\circ}$.
(A color version of this figure is available in the online journal.)

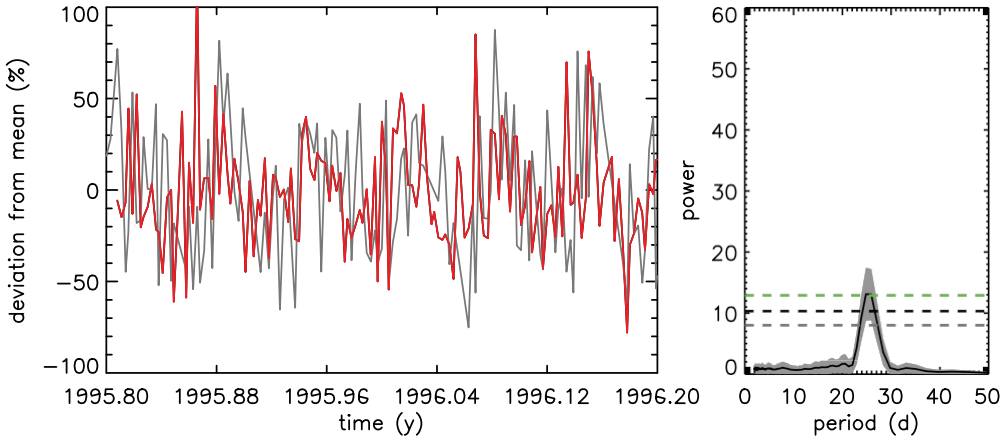

Figure 13. Same as Figure 11, but with $F_S = 3/8 \cdot F_S$.
(A color version of this figure is available in the online journal.)

observations. The right panel illustrates the corresponding Lomb frequency analysis of the noisy model data.

Since the addition of noise to the simulation data is a random process leading to different results in the Lomb analysis, the addition of noise and the Lomb analysis were performed 1000 times. The average of these frequency analyses is represented by the black curve. The gray shaded area shows the standard deviation computed from the 1000 Lomb analyses. The upper and lower gray lines indicate the 99% and 90% significance levels, respectively, while the green dashed line represents the average maximum power of the 26 day peak found in the Lomb analysis of the *Ulysses*/KET count rates. To achieve an agreement of the *Ulysses* observations and the simulation data, the peak of the 26 day variations found in the noisy simulation data has to be on the order of the green line (Lomb peak condition, LPC). The systematic variation of the modeled count rate is produced by the Schwadron–Parker HMF. Therefore, the parameters of the Schwadron–Parker HMF model have to be modified to produce a lower waviness of the HMF lines and hence satisfy the LPC.

5.1. Varying the Fisk Angle β

Burger et al. (2008) suggest that the Fisk angle β depends on the solar cycle and is less than 30° (the value assumed by Zurbuchen et al. 1997). Therefore, we computed the 7 MeV electron intensities along the *Ulysses* trajectory for lower values of β, but keeping all other parameters at the values described above. Figure 12 presents the best agreement between the simulated electron flux and the *Ulysses* observations found in this study employing $\beta = 6^{\circ}$. Here, the averaged Lomb peak of the *Ulysses*/KET analysis (dashed green line) lies close to the 26 day peak of the noisy simulated data, satisfying the LPC.

Roberts et al. (2007) state that a reduction of β by a factor of two (i.e., $\beta = 15^{\circ}$) would make the predictions of the Fisk field statistically consistent with their analysis of the HMF observations and the systematic variations of the field components become too small to be distinguishable from the noise. This work, however, shows that the Fisk angle might even be far below the upper limit found by Roberts et al. (2007).

5.2. Varying the Transition Function F_S

A second possibility is to vary the transition function F_S while keeping the Fisk angle at the original value $\beta = 30^{\circ}$. In this study, we multiplied F_S with different values $F_S = a \cdot F_S$, $a < 1$, finding $a = 3/8$ (dashed curve in Figure 2) to produce a good fit of the noisy model data to the *Ulysses* observations (Figure 13). The peak of the Lomb analysis of the simulated electron intensities fits the averaged Lomb peak of the *Ulysses* electrons, thus satisfying the LPC with the parameters employed in this investigation.

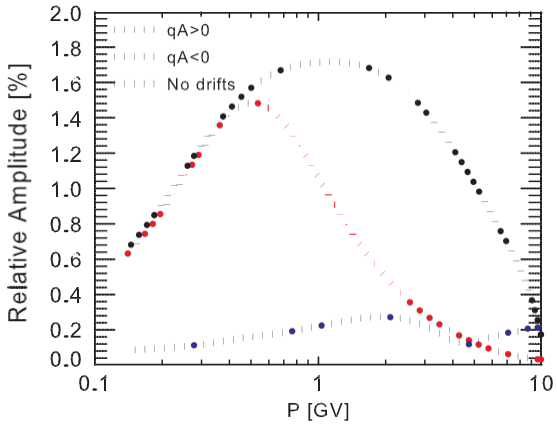

Figure 14. Proton relative amplitudes as functions of rigidity. See the text for details.
(A color version of this figure is available in the online journal.)

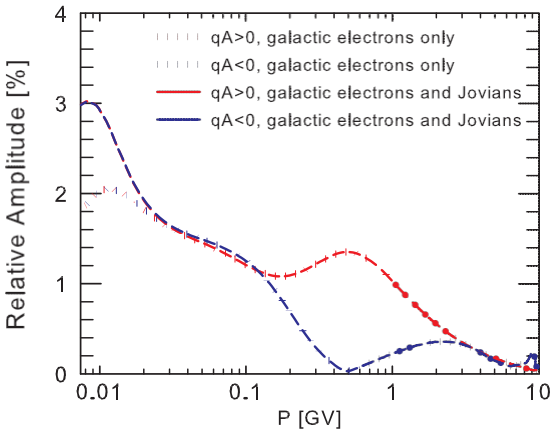

Figure 15. Electron relative amplitudes as functions of rigidity. See the text for details.
(A color version of this figure is available in the online journal.)

6. THE EFFECT OF A FISK-TYPE FIELD AND DRIFTS ON PROTON AND ELECTRON RELATIVE AMPLITUDES

Figures 5 and 6, showing the detrended *Ulysses* 2.5–7 MeV electron, and 250 MeV to 2000 MeV proton count rates, respectively, illustrate an interesting phenomenon, in that the proton variations are much smaller than those of the electrons. One could argue that this is due to the effects of drift on the protons, but it is the aim of this section to show that this is not entirely the case. Here, we briefly consider the implications of a Fisk effect reduced as indicated above on the 26 day variations of electrons relative to those of galactic protons, utilizing a three-dimensional steady-state numerical modulation code of Burger & Hattingh (1995), and including a source of Jovian electrons (see Ferreira et al. 2001a, 2001b). The Schwadron–Parker model of Hitge & Burger (2010), as in the above study, is here utilized, with a transition function reduced from that used by the above-mentioned authors by a factor of 3⁄8. The emphasis of the present study remains on the transport of low-energy electrons, but we nevertheless consider a broad range of energies here and include the effects of drift.

We here, as in Burger et al. (2008) and Engelbrecht & Burger (2010), utilize expressions for the parallel mean free path for protons and electrons based on results derived from Quasilinear theory by Teufel & Schlickeiser (2003) for the random sweeping model of dynamical turbulence (see Bieber et al. 1994). Perpendicular diffusion is here assumed to be axisymmetric and modeled utilizing the nonlinear guiding center theory (Matthaeus et al. 2003) expression derived by Shalchi et al. (2004), given for a general ratio of slab to two-dimensional turbulence in Burger et al. (2008). The turbulence quantities required by the above expressions are modeled as in Engelbrecht & Burger (2010). The drift coefficient of Burger et al. (2008) is used with a tilt angle of 10°, as only solar minimum conditions are considered. The SW speed is allowed to vary with colatitude so as to assume a value of 400 km s^{-1} in the ecliptic plane, and rising to 800 km s^{-1} over the poles. Lastly, the heliospheric boundary is set at 50 AU. This value was chosen as a compromise between the requirements of numerical stability and those of numerical resolution, and do not greatly affect the qualitative behavior of the 26 day variations, these being relative quantities. We have used the same Local Interstellar Spectrum (LIS) as used in the previous sections, with the proton LIS that was used by Burger et al. (2008).

In what follows, we consider relative amplitudes at 2 AU and 50° colatitude, where relative amplitudes are calculated as the difference between the maximum and minimum electron intensities as a function of longitude at a given radial distance and colatitude, and expressed as a percentage of the azimuthally averaged intensity at those given coordinates. We choose 50° colatitude as this is approximately where the transition function F_S is at a maximum. Note, however, that a lack of quantitative agreement as to the magnitude of relative amplitudes yielded by the VLUGR3-based model used in the previous analyses and those calculated using the three-dimensional steady-state code may be due to two reasons: the difference in diffusion coefficients used and the fact that inherently the results of the steady-state code take into account only spatial variations. The latter reason coupled with the high amount of noise on the low-energy electron data would probably also explain the lack of quantitive agreement between the results yielded by the steady-state code and the *Ulysses* data.

Figure 14 illustrates proton relative amplitudes as functions of rigidity for both $qA > 0$ and $qA < 0$ with full drift effects, and for the case where drift effects are neglected. The results are similar to those of Hitge & Burger (2010), but with an overall decrease in magnitude of the relative amplitudes, due simply to the smaller Fisk effect modeled by a reduced transition function. The inclusion of drifts leads to a decrease in relative amplitudes with increasing rigidity. Note that during $qA > 0$, the polarity pertinent to the time periods considered in the above analysis, that the relative amplitude at 250 MeV ($\sim$1.1 MV) is $\sim$1.4%, while at 2000 MeV ($\sim$2600 GV), it is $\sim$0.3%. For the no drift case, at 250 MeV the relative amplitude assumes a value of $\sim$1.8%, while at 2000 MeV it assumes a value of $\sim$1.5%, implying a drop in the relative amplitudes due to drifts at these energies by factors of $\sim$1.3 and $\sim$5.0, respectively.

When the electron relative amplitudes are considered as functions of rigidity in Figure 15, we see that for both Jovians and galactics, as well as for galactics only, a steep drop-off occurs in the relative amplitudes with decreasing rigidity. This behavior may be due to diffusion parallel to the magnetic field lines being a dominant factor. At the smallest rigidities, the inclusion of a Jovian source yields greater relative amplitudes than when galactics alone are considered, as can be expected from the addition of a source of low-energy electrons, and indicative of the enhanced latitudinal transport of Jovian electrons implicitly in the field line structure of Fisk-type fields. When a Jovian source

is included, the Schwadron–Parker model with reduced Fisk effect yields results qualitatively in agreement with the *Ulysses* data presented above in that the relative amplitudes of these electrons are greater than those of the 250 MeV to 2000 MeV protons, so that at 7 MeV (∼7 MV) during $qA < 0$, the relative amplitude is ∼3.0%, a factor of ∼2.1 higher than the 250 MeV proton value, and ∼10.0 times that of the 2000 MeV proton relative amplitude, when the effects of drift on the galactic protons are included. This phenomenon is not solely due to the reduction of the proton relative amplitudes at these energies due to drifts, because even when drift effects are ignored, the 7 MeV electron relative amplitudes are still a factor of ∼1.7 greater than the 250 MeV proton relative amplitudes, and a factor of ∼2.0 greater than the 2000 MeV proton relative amplitudes. When only galactic electrons are considered, the relative amplitudes at 7 MeV assume a value of ∼1.8%, similar to those of the protons at 250 MeV, and differing by a factor of ∼1.3, whereas when compared with the relative amplitudes of 2000 MeV protons, the values differ by a factor of ∼6.0, assuming full drift effects. Neglecting drift, however, alters the picture somewhat, in that the 7 MeV electron relative amplitudes are almost the same as the proton relative amplitudes at 250 MeV, and differ by only a factor of ∼1.2 at 2000 MeV. This implies that this phenomenon is due to the presence of Jovian electrons at higher latitudes and, as no ad hoc enhanced perpendicular diffusion is assumed in this study, that the Jovian electrons would have reached these higher latitudes by means of diffusion parallel to the Schwadron–Parker field lines.

7. SUMMARY AND CONCLUSIONS

In the present study, the investigation of the electron intensities in a Fisk-type HMF became possible for the first time in a three-dimensional time-dependent model. Therefore, the 2.5–7 MeV electron observations at high heliolatitudes could be used as a remote sensing method for the HMF structure. To achieve this, the Schwadron–Parker hybrid HMF model (Hitge & Burger 2010) was chosen as the most adequate representation of a Fisk-type HMF today. Simulations of the 7 MeV electron flux in the heliosphere reveal 26 day variations at mid to high latitudes in the inner heliosphere. The analysis of the *Ulysses*/KET 2.5–7 MeV electron data leads to the conclusion that a 26 day variation can also be found in the electron count rate at mid to high latitudes of the *Ulysses* trajectory between 1995.6 and 1996.3. A further analysis of proton and SW speed data could exclude CIRs and the SW as possible causes of the electron variations. These results lead to the conclusion that the HMF structure is actually Fisk-like at the corresponding latitudes during the considered period of time, a finding which might be impossible to derive from the available magnetic field observations due to the fact that the systematic variations of the magnetic field components predicted by the Fisk field are too small to exceed the noise (Roberts et al. 2007).

In addition, consistent parameter values for the Fisk theory could be deduced from a comparison of model computations and *Ulysses*/KET measurements showing that lower parameter values lead to a good agreement between the *Ulysses*/KET electron observations and the simulation data. The relative amplitudes calculated for protons with the Schwadron–Parker field with the more realistic Fisk-field parameters presented above are smaller than those calculated by Hitge & Burger (2010), but are qualitatively similar as functions of rigidity. When electrons are considered, at the lowest rigidities the effect of the Jovian source is clearly seen, with higher relative amplitudes than when only galactic electrons are considered, due to enhanced access of Jovian electrons to the polar regions. When the modeled relative amplitudes for 7 MeV electrons (including a Jovian source) are compared with those of 250–2000 MeV galactic protons, the electron amplitudes are greater than those of the protons, even when the effects of drift are neglected, in qualitative agreement with the *Ulysses* data presented in this study.

The investigation of the two extreme cases of a reduced Fisk effect leading to similar results suggests that a reduction of both, β and F_S, will lead to the most realistic parameter set for the Fisk theory. Burger et al. (2008) assume β to lie around 12°–13° between 1995.6 and 1996.3. Combining their approximation with a reduced transition function will still explain the 7 MeV electron variations seen by *Ulysses* and give an accurate description of the HMF during solar minimum conditions.

The finding of this investigation is consistent with the study of Lionello et al. (2006), which confirms the principle idea of Fisk-type fields with their MHD model, but calls for refinements of the Fisk theory, as well as the study of Roberts et al. (2007), which concludes that—if the Fisk theory is applicable—the parameters of the theory were overestimated so far finding an upper limit of 15° for the Fisk angle β. The parameter values of $\beta \approx 12^\circ$–13° with a reduced transition function F_S found in this work reduce the Fisk effect in the HMF model even below the postulation of Roberts et al. (2007).

The consequences of the results found in this work will be discussed in a subsequent paper.

We thank the referee for his/her constructive comments on this paper.

The *Ulysses*/KET project is supported under grant 50 OC 0902 by the German Bundesministerium für Wirtschaft through the Deutsches Zentrum für Luft- und Raumfahrt (DLR). This work benefited from the support from the German Bundesministerium für Bildung und Forschung (BMBF project SUA 08/011) and from the Deutsche Forschungsgemeinschaft (DFG project Heliocauses). The German-South African collaboration is supported by the DLR under grant SUA 07/013 and under the SA-Germany Science, Research and Technology Cooperation Agreement, and partial funding by the South African National Research Foundation (NRF).

This work profited from the discussions with the participants of the ISSI team meeting "Transport of Energetic Particles in the Inner Heliosphere."

REFERENCES

Bieber, J. W., Matthaeus, W. H., Smith, C. W., et al. 1994, ApJ, 420, 294
Blom, J. G., & Verwer, J. G. 1994, Appl. Numer. Math., 16, 129
Blom, J. G., & Verwer, J. G. 1996, ACM Trans. Math. Softw., 22, 329
Box, G. E. P., & Muller, M. E. 1958, Ann. Math. Stat., 29, 610
Burger, R. A., & Hattingh, M. 1995, Astrophys. Space Sci., 230, 375
Burger, R. A., & Hitge, M. 2004, ApJ, 617, L73
Burger, R. A., Krüger, T. P. J., Hitge, M., & Engelbrecht, N. E. 2008, ApJ, 674, 511
Drury, L. O., & Völk, J. H. 1981, ApJ, 248, 344
Dunzlaff, P., Heber, B., Kopp, A., et al. 2008, Ann. Geophys., 26, 3127
Dunzlaff, P., Kopp, A., & Heber, B. 2010, J. Geophys. Res. (Space Phys.), 115, A10106
Engelbrecht, N. E., & Burger, R. A. 2010, Adv. Space Res., 45, 1015
Ferrando, P. 1999, Proc. 26th ICRC (Salt Lake City), 7, 135
Ferreira, S. E. S., Potgieter, M. S., Burger, R. A., Heber, B., & Fichtner, H. 2001a, J. Geophys. Res., 106, 24979
Ferreira, S. E. S., Potgieter, M. S., Burger, R. A., et al. 2001b, J. Geophys. Res., 106, 29313

Ferreira, S. E. S., Potgieter, M. S., Heber, B., & Fichtner, H. 2003, Ann. Geophys., 21, 1359
Fichtner, H., Potgieter, M. S., Ferreira, S. E. S., Heber, B., & Burger, R. A. 2001, Proc. 27th ICRC (Hamburg), 9, 3666
Fisk, L. A. 1996, J. Geophys. Res., 101, 15547
Forsyth, R. J., Balogh, A., & Smith, E. J. 2002, J. Geophys. Res. (Space Phys.), 107, 1405
Gosling, J. T., & Pizzo, V. J. 1999, Space Sci. Rev., 89, 21
Heber, B., Bothmer, V., Dröge, W., et al. 1997, in Correlated Phenomena at the Sun, in the Heliosphere and in Geospace, ed. A. Wilson (ESA-SP 415; Noordwijk: ESA), 331
Hitge, M., & Burger, R. A. 2010, Adv. Space Res., 45, 18
Jokipii, J. R., Kóta, J., Giacalone, J., Horbury, T. S., & Smith, E. J. 1995, Geophys. Res. Lett., 22, 3385
Kissmann, R. 2002, Diploma thesis, Ruhr-Universität Bochum
Kissmann, R., Fichtner, H., & Ferreira, S. E. S. 2004, A&A, 419, 357
Kissmann, R., Fichtner, H., Heber, B., Ferreira, S. E. S., & Potgieter, M. S. 2003, Adv. Space Res., 32, 681
Kóta, J., & Jokipii, J. R. 1995, Science, 268, 1024
Kunow, H., Dröge, W., Heber, B., et al. 1995, Space Sci. Rev., 72, 397
Kunow, H., Lee, M. A., Fisk, L. A., et al. 1999, Space Sci. Rev., 89, 221
Lange, D., Fichtner, H., & Kissmann, R. 2006, A&A, 449, 401
Langner, U. W., de Jager, O. C., & Potgieter, M. S. 2001, Adv. Space Res., 27, 517
Lario, D., & Roelof, E. C. 2007, J. Geophys. Res. (Space Phys.), 112, A09107
Lionello, R., Linker, J. A., Mikić, Z., & Riley, P. 2006, ApJ, 642, L69
Lomb, N. R. 1976, Ap&SS, 39, 447
Matthaeus, W. H., Qin, G., Bieber, J. W., & Zank, G. P. 2003, ApJ, 590, L53
McKibben, R. B., Connell, J. J., Lopate, C., Simpson, J. A., & Zhang, M. 1996, A&A, 316, 547
Miyake, S., & Yanagita, S. 2008, Proc. 30th ICRC, 1, 445
Ness, N. F., & Burlaga, L. F. 2001, J. Geophys. Res., 106, 15803
Parker, E. N. 1958, ApJ, 128, 664
Parker, E. N. 1965, Planet. Space Sci., 13, 9
Potgieter, M. S. 1996, J. Geophys. Res., 101, 24411
Potgieter, M. S. 1998, Space Sci. Rev., 83, 147
Potgieter, M. S., & Ferreira, S. E. S. 1999, Adv. Space Res., 23, 463
Roberts, D. A., Giacalone, J., Jokipii, J. R., Goldstein, M. L., & Zepp, T. D. 2007, J. Geophys. Res. (Space Phys.), 112, A08103
Scherer, K., Fichtner, H., Effenberger, F., Burger, R. A., & Wiengarten, T. 2010, A&A, 521, A1
Schou, J., Antia, H. M., Basu, S., et al. 1998, ApJ, 505, 390
Schwadron, N. A., & McComas, D. J. 2003, Geophys. Res. Lett., 30, 1587
Shalchi, A., Bieber, J. W., & Matthaeus, W. H. 2004, ApJ, 604, 675
Simpson, J. A., Anglin, J. D., Bothmer, V., et al. 1995a, Science, 268, 1019
Simpson, J. A., Connell, J. J., Lopate, C., McKibben, R. B., & Zhang, M. 1995b, Geophys. Res. Lett., 22, 3337
Simpson, J. A., Zhang, M., & Bame, S. 1996, ApJ, 465, L69
Teufel, A., & Schlickeiser, R. 2003, A&A, 397, 15
Zhang, M., McKibben, R. B., Simpson, J. A., et al. 1995, J. Geophys. Res., 100, 19497
Zurbuchen, T. H., Schwadron, N. A., & Fisk, L. A. 1997, J. Geophys. Res., 102, 24175